Eindhoven University of Technology

MASTER

Electrochemical Neuromorphic Organic Devices

Schilp, Winston

Award date:
2021

Link to publication

MASTER THESIS

Electrochemical Neuromorphic Organic Devices

Eindhoven, July 20, 2021

Winston Schilp, BSc
Supervisors: dr. A.J. Kronemeijer, Prof. dr. G.H. Gelinck

Electrochemical Neuromorphic Organic Devices (ENODes) are akin to analogously programmable transistors with memory. In this report, they rely on the property of PEDOT:PSS to store both ionic- and electronic charge, which also changes its conductivity. The viability of these ENODes with prospect to application in artificial neural network hardware is investigated. A successful transition from devices with liquid electrolyte to encapsulated solid-state electrolyte is described, as well as an investigation into the scalability of the devices. We found that smaller devices have shorter programming times, but also shorter state retention times. The hypothesized mechanism for state instability - the unintended diffusion of cations - is researched, along with measures to prevent this.

Sending current pulses instead of voltage pulses to the gate have been found to make the programmable range more linear and therefore easier to program.

Contents

Chapter 1

Introduction

Artificial Neural Networks (ANN's) have been a scientific field of great interest for the last decennia, due to their central role in many machine learning applications. These applications include regression analysis[1], classification[2], data processing[3] and robotics[4].

Generally speaking, training ANN's is quite time-, energy- and data intensive [5]. 'Classical' computers built according to the von Neumann architecture are limited by the design choice of using the same bus (data channel) for the program memory and data memory and are therefore sub-optimally designed for processing the vast amounts of data that ANN's can require. This limit is also called the 'von Neumann bottleneck'.

Google is already invested in designing hardware specifically designed for handling machine-learning related problems[6]. One example of the use of these Tensor Processing Units (TPU's) is in the game computer AlphaGo, used in the match against the Go world champion Lee Sedol. Of course, these TPU's are also useful in the earlier mentioned machine learning applications.

This report focuses on a new and upcoming application in the field of organic electronics. More specifically, devices that boast both a variable resistance and memory. This allows them to function as weights in ANN's (more about this in chapter 2).

These devices, called Electrochemical Neuromorphic Organic Devices (ENODes), come with a few benefits that are common in organic electronics, such as mechanical flexibility and chemical adaptability. On top of that, these devices require very little energy to switch states (<10 pJ for 10^3 μm^2)[7].

A lot of work has already been done on these devices [7][8][9][10][11][12] and on similar devices that share the majority of their physics with the ENODes, but are more designed towards low-concentration solution detection [13][14][15][16][17]. These devices are called organic

electrochemical transistors (OECTs) and they use the same detection principle of a solvent changing the conductance of an electrical channel, which determines the electrical signal measured. Using an electrolyte to tune the ion concentration in such a channel in a controlled fashion allows for an energy-efficient signal manipulation.

This, in context of ENODes, is elaborated on in chapter 2. Chapter 3 will discuss the measurement setups used and the production methods, chapter 4 will discuss the experiments and their findings, which will be concluded in chapter 5.

Chapter 2

Theory

2.1 ENODes

2.1.1 Function of an ENODe

Electrochemical Neuromorphic Organic Devices (ENODes) are three-terminal devices that are somewhat reminiscent of transistors. The locations and names of these terminals can be found in Figure 2.1a and -b, together with the device design.

   The idea of an ENODe is that the channel has a variable conductance, which can be programmed by applying a voltage at the gate. Furthermore, when the programming of the ENODe is finished, the conductance level of the channel should remain constant until further programming.

2.1.2 Physics of an ENODe

During programming, the gate potential displaces ions through the electrolyte. In the case of a positive gate potential, ions are pushed out of the gate PEDOT:PSS into the electrolyte and subsequently from the electrolyte into the channel PEDOT:PSS, as can be seen in Figure 2.1a. The channel is the patch of PEDOT:PSS between the source and drain and the conductivity of the patch determines the effect on the electrical signal that is sent through the device. In the case of a negative potential, the reverse happens. It is important to note that only the cation movement is of importance. The electrolyte anions do not enter the channel.

   Now the tuning mechanisms of the PEDOT:PSS in the channel during programming will be discussed. The structural formula of PEDOT and PEDOT:PSS can be seen in Figure 2.2. The ionic bond between the positive PEDOT and negative PSS is displayed in red. In the conductive
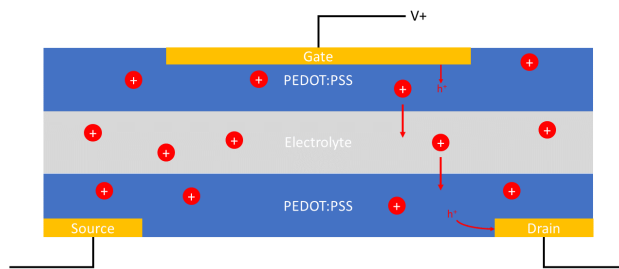
(a) Programming process of an ENODe with positive gate pulses. The positive gate voltage pushes cations through the electrolyte into the channel between the source- and drain terminal. This reduces the channel PEDOT:PSS by pushing out a hole through the terminals.
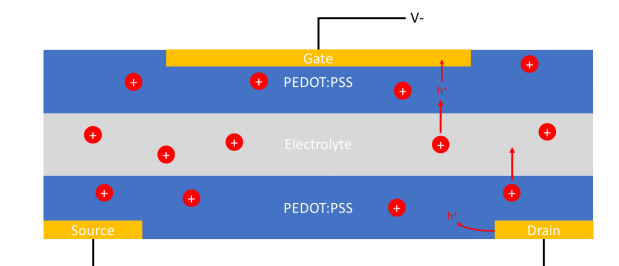
(b) Programming process of an ENODe with negative gate pulses. Here the reverse happens from Figure 2.1a.

Figure 2.1

state, displayed in Figure 2.3a, when the double bonds of PEDOT become single bonds to compensate for the PSS, which now lacks protons and is therefore negative, holes can hop between the PEDOT monomers over the chain of double bonds. Once a cation enters the channel from the electrolyte, it compensates the negative PSS, screening it from the PEDOT. The PEDOT then draws in electrons from its environment - mostly from the terminals - and restores its double bonds. This process can be seen in Figure 2.3b. The double bonds are very rigid and thus inhibit hole/electron conductance. This is how the channel conductivity is programmed by moving cations through the electrolyte with the gate potential. So, a positive gate potential reduces the channel and lowers its conductance.
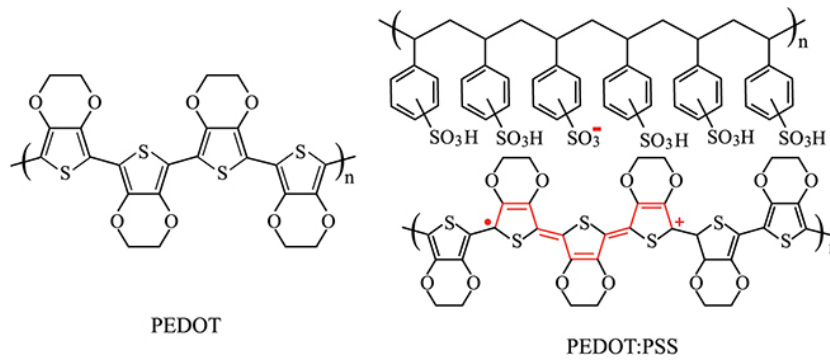
Figure 2.2: The structural formula of PEDOT:PSS. The part in red indicates the charged parts that form the ionic bonds in PEDOT:PSS. Source: [18]

2.1.3 PEDOT:PSS capacitance

As mentioned before, PEDOT:PSS has a special property of being able to store both ionic- and electronic charge. The structural formula given, however, does not disclose everythingh about its morphology. The PEDOT and PSS are clustered in grains [19], as can be seen in Figure 2.4. The grains allow electric double layers, a mechanism also seen in superconductors, where the double layers form on the surfaces of porous electrodes. Here, however, the double layers are formed on the interfaces between grains.
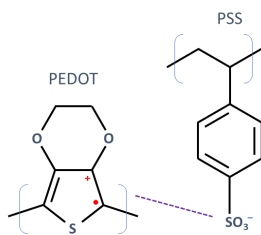
(a) Uncompensated PEDOT:PSS. The positive hole is displayed in red, the negative SO_3^- The ionic bond between the ionomers is displayed in purple.
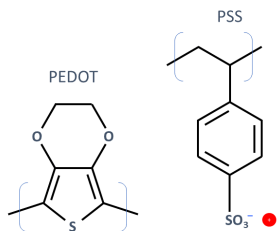
(b) Compensated PEDOT:PSS. The cation in red was provided by the electrolyte and compensates the negative SO_3^-, which breaks the ionic bond and restores the non-conductive double bond in the PEDOT.

Figure 2.3
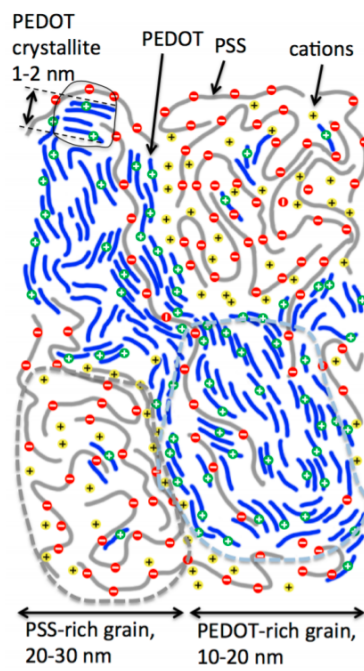
Figure 2.4: Schematic representation of the grain structure in PEDOT:PSS. Source: [19]

2.2 Artificial Neural Networks

Developing a piece of technology should always be done with a goal in mind. The most obvious application of ENODes is integration in neural network hardware. This section will elaborate on that application.

A neural network is a set of nodes and connections, organized in layers, which can be seen in Figure 2.5. These nodes contain a number, typically between 0 and 1 and the connection determines the effect of the number on the node that it is connected to in the next layer according to this formula:

$$a^{(L)} = f(w^{(L)}a^{(L-1)} + b^{(L)}) \tag{2.1}$$

where

- $a^{(L)}$ indicates the inputs of the nodes in layer L in the form of an array.

- f indicates an activation function, which maps $\mathbb{R}1$ onto the interval [0,1]. This function works on every element of the resulting array on the right hand side, rather than the array as a whole.

- $w^{(L)}$ is the weight matrix. Element $w_{jk}^{(L)}$ indicates the effect of node k in layer $L-1$ on node j in layer L. This factor of the multiplication between these elements is also called the weight.

- $b^{(L)}$ is the bias array. This adds a value to each node and allows for tweaking the treshold value for when a node should activate a subsequent node.

The application of ENODes would be as the aforementioned weights. One way this could be implemented is to implement them in a crossbar array, as displayed in Figure 2.6. The input signals would go in the vertical lines and the output signal would come out of the horizontal ones or vice versa. The ENODes can be programmed to change the resistance of the connection between the perpendicular lines, thus dictating the output signal as a result of an input signal.
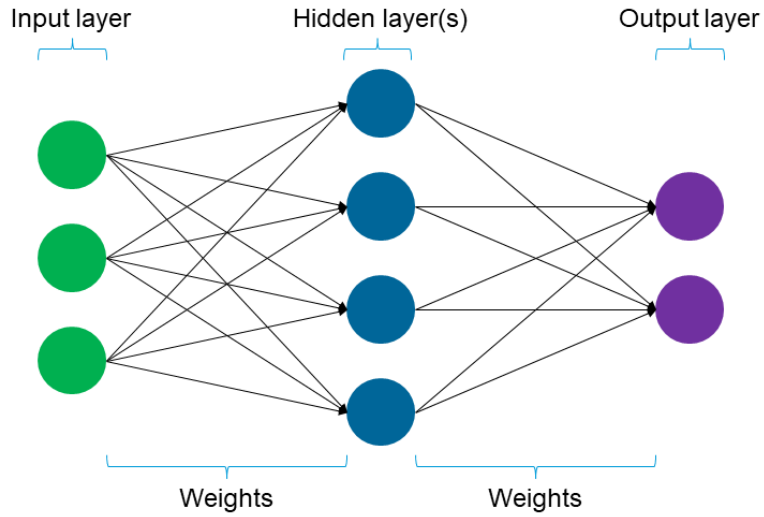
Figure 2.5: A schematic representation of a neural network. The colored circles represent the nodes, organized in layers. The signals pass through the weights from left to right.
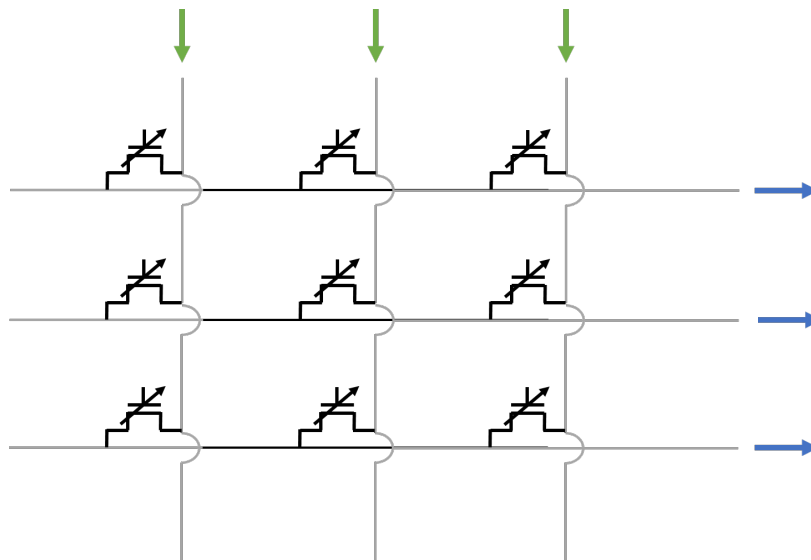
Figure 2.6: A schematic representation of a crossbar array. In analogy to Figure 2.5, the green input signals represents three nodes from the input layer and the blue output signals represent three nodes in the hidden layer. The black icons are ENODes and their programmed state determines the transfer of voltage from the input- to the output lines.

Chapter 3

Methods

3.1 Sample production

The substrate used for the samples is a 6x6 inch square glass plate from Eagle XG®. The photo-resist, developer and stripper are part of a kit from the company Orthogonal Inc. The sample design can be found in Figure 3.2. The process for producing the ENODes is as follows:

1. Sputter titanium on the glass, followed by a layer of gold.

2. Cover the metal patterns in photo-resist and strip away the rest.

3. Spin-coat and develop photo-resist on the entire plate, but etch wells into the photoresist for the gate- and channel PEDOT:PSS.

4. Pre-wet the substrate, spin the water off and then spincoat the PEDOT:PSS at 1050 rpm. This yields layers of about 100 nm thick.

5. Pattern the PEDOT:PSS with photo-resist and etch away the rest.

6. Etch away the photo-resist on the PEDOT:PSS with oxygen plasma.

From this point on, the samples are already programmable when an electrolyte like salinated water is placed over the PEDOT:PSS patches. A picture can be seen in Figure 3.3. Samples with a solid-state gel electrolyte require the following steps:

1. Mix, by weight, %4.4 PVDF-HFP, %17.6 EMIM:TFSI, %78 acetone for at least 30 minutes at 40 degrees Celsius.

2. Deposit the gel on the sample, either directly by spincoating at 600 rpm for 30 seconds or indirectly by pouring it in a mold, cutting and pasting it onto the ENODes. Spincoating yields a layer of about 7 micron thick

The structural formulas of EMIM:TFSI and PVDF-HFP can be seen in Figure 3.1a and b. EMIM:TFSI is an ionic liquid that can be contained in a cross-linked network of PVDF-HFP.
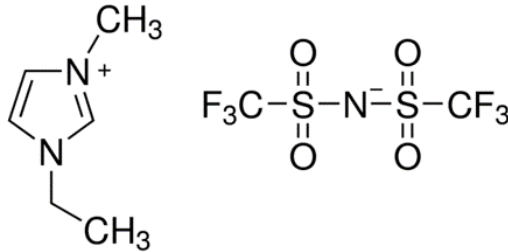
(a) Structural formula of EMIM:TFSI.
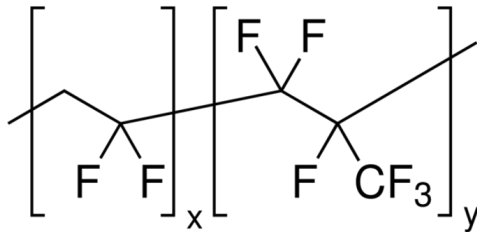
(b) Structural formula of PVDF-HFP.

Figure 3.1

3.2 Measurement setup

The samples are measured in a probe station, protected by a grounded Faraday cage. Depending on the measurement, the following devices were used as source- and measurement units:

- Keithley 2612A

- Agilent 4155A

There are two setups with an Agilent 4155A. One is in ambient atmosphere, one is in a water- and oxygen controlled glove box with setpoints of less than 0.1 ppm of both species. The devices were connected to the probes with either coax- or triax cables.

Figure 3.2: Design of the samples. Only the six vertically oriented samples are used in this report. Pink represents TiAu, blue is holes in the photoresist layer for contact with either probes or PEDOT:PSS, and green is PEDOT:PSS. Note that the PEDOT:PSS channel between the source- and drain lead changes in size for each of these six ENODes.

Figure 3.3: Picture of (part of) a produced sample. The sample is 2x2 cm.

3.3   Thin Film Transistor measurements

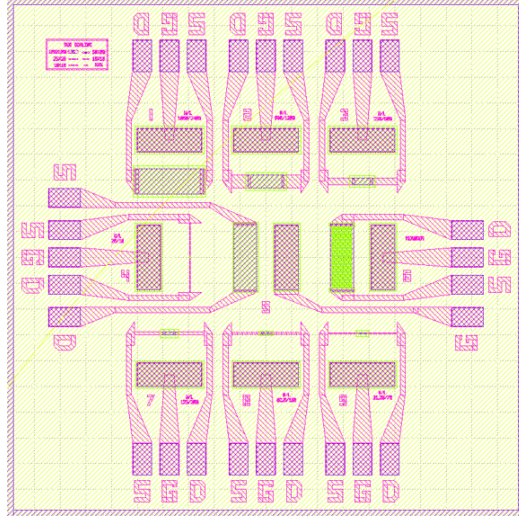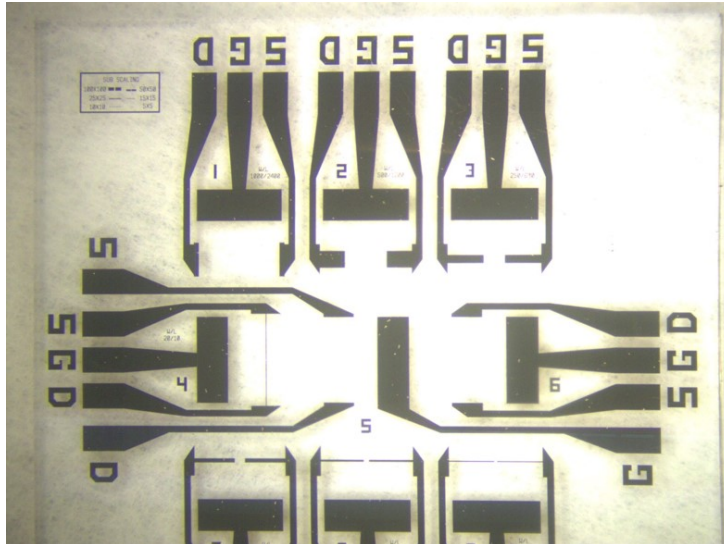In one of the experiments, a Thin Film Transistor (TFT) was placed before the gate of the ENODe to regulate the in- and outflow of charge. The electric scheme can be seen in Figure 3.4 and the actual setup in Figure 3.5. The on- and off voltages of the TFT are 10 and -10V, respectively. The transfer curve of the TFT can be found in Figure 6.1. These gate voltages switch the TFT between a resistance of 100 kΩ and 1 TΩ.
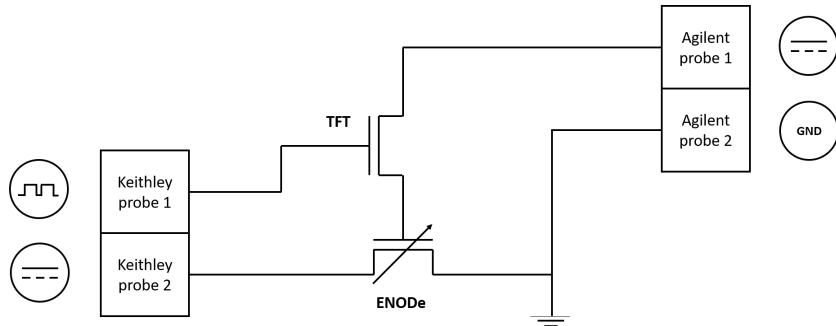
Figure 3.4: Schematic display of the TFT-ENODe setup. Keithley probe one is responsible for opening and closing the TFT before the ENODe. Agilent probe one actually provides the charge for the ENODe gate. Keithley probe two acts as a source-measurement unit for the ENODe and Agilent probe two acts as a common ground between the two devices.

3.4   Device layout

In the specific devices we work with, there are six ENODes, which can be seen in Figure 3.2.   Each ENODe has the same amount of gate PEDOT:PSS, but by design, both the width and the length of the channel PEDOT:PSS halve with each subsequent ENODE. The idea is that the conductivity of the channel should remain the same if the channel area decreases, because the aspect ratio and therefore the sheet resistance stays the same. The aspect ratio of all these samples is width/length = 1/2.4. By approximation, the gate and channel PEDOT:PSS patches can be seen as capacitors for ionic charge. More specifically, they can be seen as a pair of capacitors in series. The capacitance of a PEDOT:PSS patch scales, again by approximation, linearly with its volume [19]. Since the PEDOT:PSS layers are all spin-coated, they should have roughly the same thickness of roughly 100 nm. Therefore, the capacitance of each subsequent channel decreases by a fourth. The gate and channel of the first ENODe are the
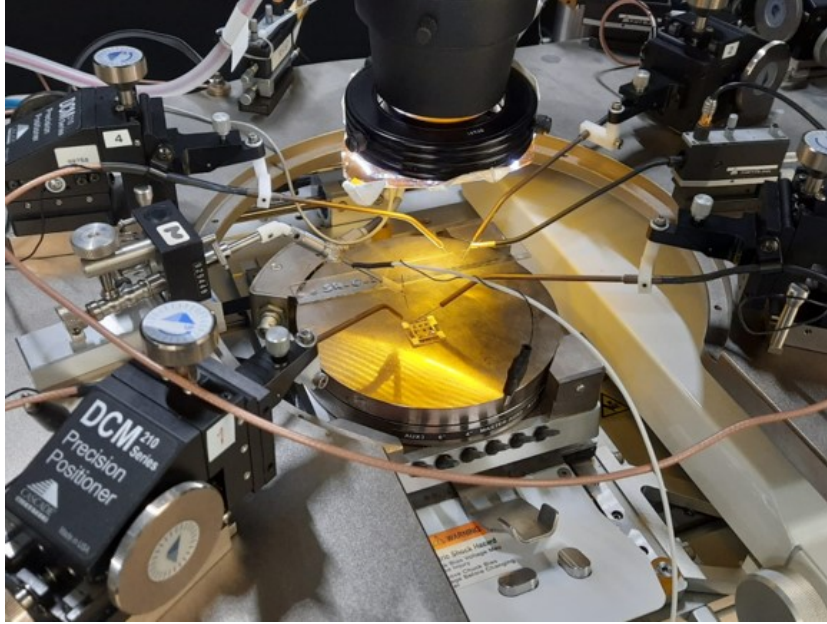
Figure 3.5: Photo of the TFT setup. Four probes are used to build the scheme in Figure 3.4 and two to connect the TFT and ENODe.

same in size, so the relative capacitance of each subsequent ENODe with respect to the first one is smaller. We can formulate the ratio of the total capacitance of ENODe N with respect to the largest ENODe.

The total capacitance of a single ENODe is the replacement capacitance of two capacitors in series.

$$C_{ENODe} = \frac{C_{gate} * C_{channel}}{C_{gate} + C_{channel}} \tag{3.1}$$

In the first ENODe, the C_{gate} and $C_{channel}$ are roughly the same. With each subsequent ENODe, the channel decreases a factor 4, so for the Nth ENODe:

$$C_N = \frac{C_{gate} * (\frac{1}{4})^N C_{gate}}{C_{gate} + (\frac{1}{4})^N C_{gate}}, \tag{3.2}$$

which brings us to

$$\frac{C_N}{C_0} = \frac{2}{1 + 4^N}. \tag{3.3}$$

Chapter 4

Results

4.1 The first attempts

Ideally, an ENODe would program linearly with the amount of gate pulses. It would hold its conductance state indefinitely and it would have a large, if not infinite, range of conductance states to choose from. The first attempts used water as an electrolyte, because this was easily accessible and proven to work in literature [15] [10], at least with the addition of NaCl, though regular water also works. In order to prevent electrons from flowing out of the gate after programming, a $10\text{M}\Omega$ resistor was added before the gate.

The first results, shown in Figure 4.1 and -b showed some imperfections. The most problematic of which is that the source-drain current has the tendency to decay back to an equilibrium level. This decay back to the equilibrium state will from now on be called relaxation. The further the channel conductance state is out of equilibrium, the more rapid it wants to relax. It is possible to reprogram the device every so often to maintain its state, but it is undesirable to do so because it costs time and energy. Furthermore, the device does not program linearly, as is evident from the curvature in the plot. Programming linearly is desirable because it allows for a very simple and predictable programming scheme, which saves necessary hardware to control the ENODes in contrast to nonlinear writing schemes. For the same reason it is undesirable that the the programming is asymmetrical, meaning that a pulse of certain voltage and duration does not yield the opposite change in conductance as a similar pulse of opposite sign. In the plot, the final state is quite different from the intial state, even though the same amount of pulses of opposite sign was supplied. There is a small linear regime in the program space of the ENODe. In the future it might be desirable to increase this linear regime to allow for more states.

The first line of attack to eliminate the most cumbersome imperfection, state relaxation, is to block the loss of charges out the gate. The 10MΩ resistor allows for these charge leaks, at least more than a larger resistor. So the resistor was replaced with a Thin Film Transistor (TFT). This resulted in the plot seen in Figure 4.2a and -b. Even with a TFT resistance of 1TΩ in the closed state the ENODes still relax. As expected, the states are more stable, but the relaxation remains a problem.

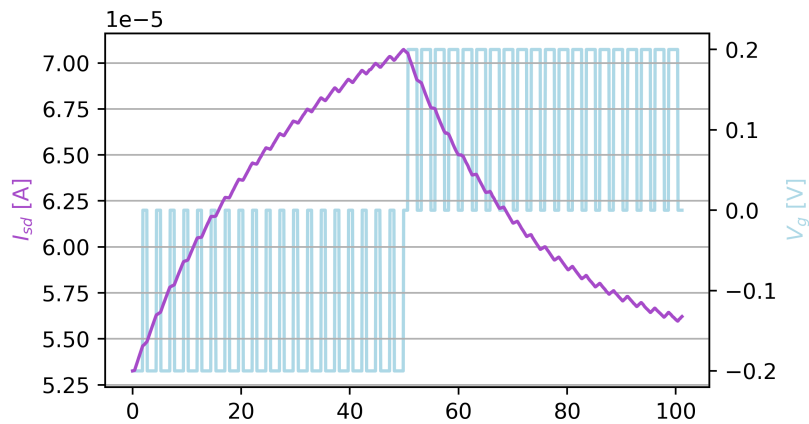Figure 4.1: Programming response of an ENODe with channel surface area of 2.4mm^2 to pulses of 0.2V and -0.2V. A 10MΩ resistor was placed between the source unit and the gate. Tha channel voltage was 0.2V.
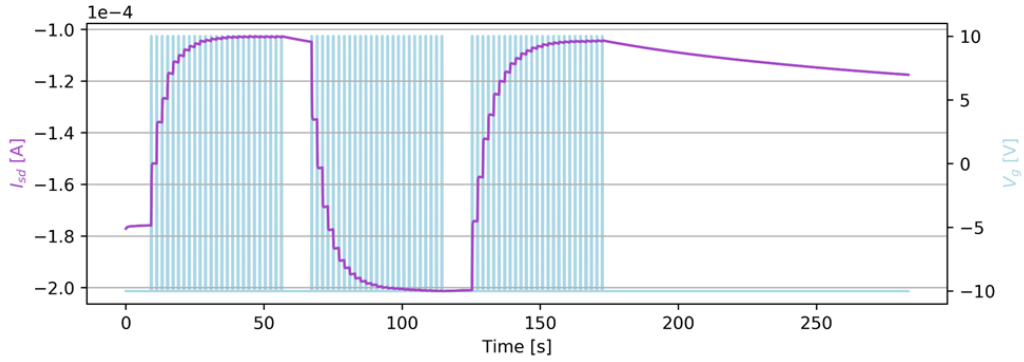
(a) Plot of the programming measurement with a TFT before the gate, using the setup described in Figure 3.4. This measurement measures the effect of gate pulses on the ENODe channel current. The three sets of pulse trains are respectively positive, negative and positive pulses of (-)0.2V through an open TFT with a resistance of about 10kΩ. The pulses are 3ms on and 9ms off. The channel voltage is 0.2V.
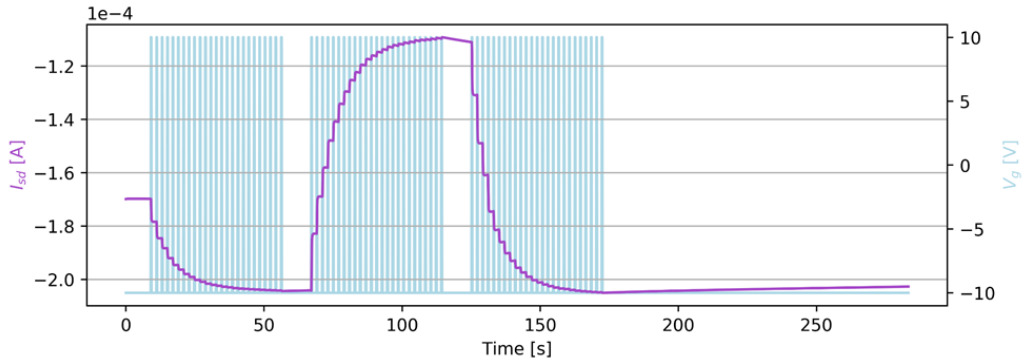
(b) Plot of the programming measurement with an TFT before the gate, using the setup described in Figure 3.4. This measurement measures the effect of gate pulses on the ENODe channel current. The three sets of pulse trains are respectively negative, positive and negative pulses of (-)0.2V through an open TFT with a resistance of about 10kΩ. The pulses are 3ms on and 9ms off. The channel voltage is 0.2V.

Figure 4.2

One definitive check to see if charges leave through the gate probe is to disconnect the gate probe altogether after programming. This still yields relaxation issues, so using TFT's with higher resistance will not result in

more stable states.

We hypothesize that this is due to back-diffusion of cations in- and out the gate- and channel PEDOT:PSS. Even though the diffusion of a cation would leave an uncompensated hole in the channel, this hole could be compensated by an electron that leaks in through one of the terminals or the environment.

One way to test this back-diffusion hypothesis is to increase the sample temperature with each relaxation measurement. This relaxation roughly follows an exponential decay, so in this test, the decay time τ of an exponential with the form

$$y(t) = Ae^{-\frac{t}{\tau}} + B \tag{4.1}$$

was plotted against temperature. This plot can be seen in figure Figure 4.3. As expected, an increased temperature accelerates the relaxation, which is in line with the hypothesis of diffusion. This is useful information with the end goal in mind. Even well-cooled computer hardware can easily reach 60 degrees Celsius and higher temperatures are by no means an exception, so it is important that the possible effects of such temperatures on these devices are considered. What enforces this idea is that, as can be seen in Figure 4.4a, the signal stops decaying after the electrolyte has been removed so no back-diffusion can happen. In this case, the water droplet used as electrolyte and ion bridge evaporated.
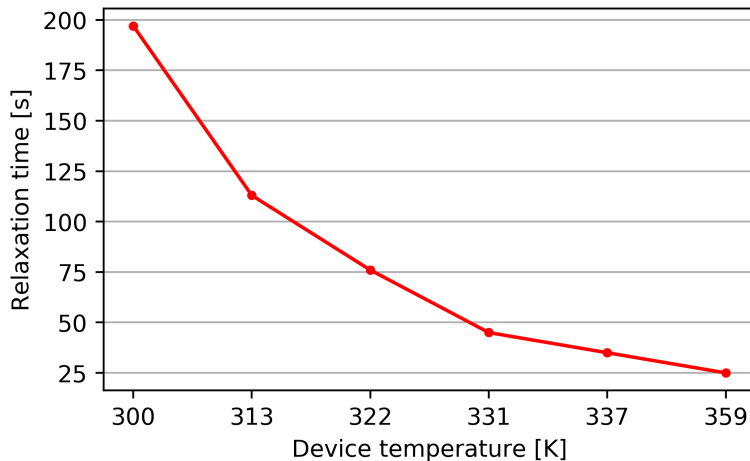
Figure 4.3: Plot of relaxation time with respect to electrolyte temperature. The devices were charged at 0.2V for 10 seconds. The gate was then disconnected. The temperature was controlled with a combination of a hotplate and a thermocouple thermometer.

Evidently, the inhibition of this back-diffusion should stabilize the devices. One more controlled way to do this is to lift the source- and drain electrodes in between measurements. If terminal charges are not allowed to flow back into the channel, back-diffusion of cations should be inhibited because for every cation diffusing out of the channel, an uncompensated hole is left in a PEDOT molecule, moving the channel further out of charge neutrality. Figure 4.4a and b show that removing the source- and drain terminals does indeed prolong the lifetime of the programmed state over three times, as it takes three times longer to decay $8*10^{-6}A$ when the channel is deprived from terminal charges. The way this could be implemented in hardware is by placing TFT's behind all three terminals and closing them when no programming or reading needs to be done.
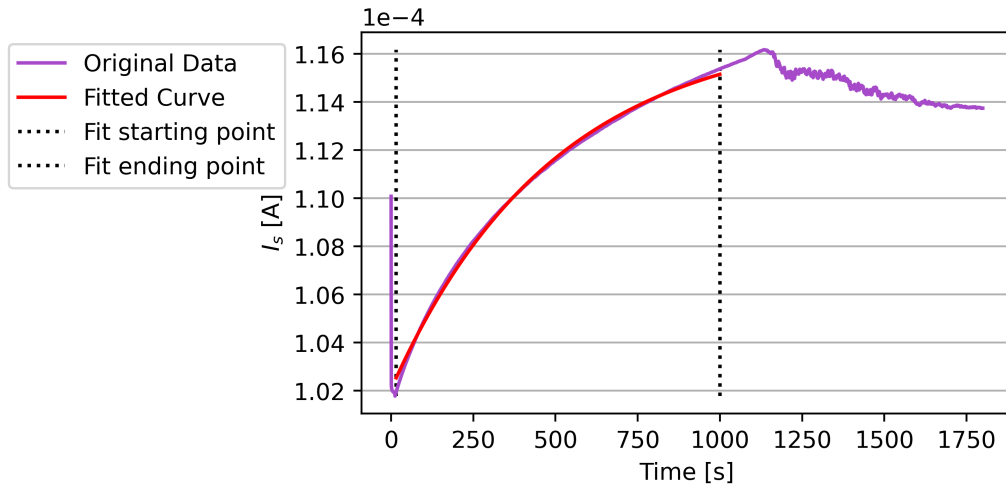
(a) A regular decay of an ENODe with a channel surface area of 2.4mm^2. After the endpoint of the fit, the water droplet used in this experiment evaporated. The device was charged at 0.2V for 10 seconds and the gate electrode subsequently disconnected.
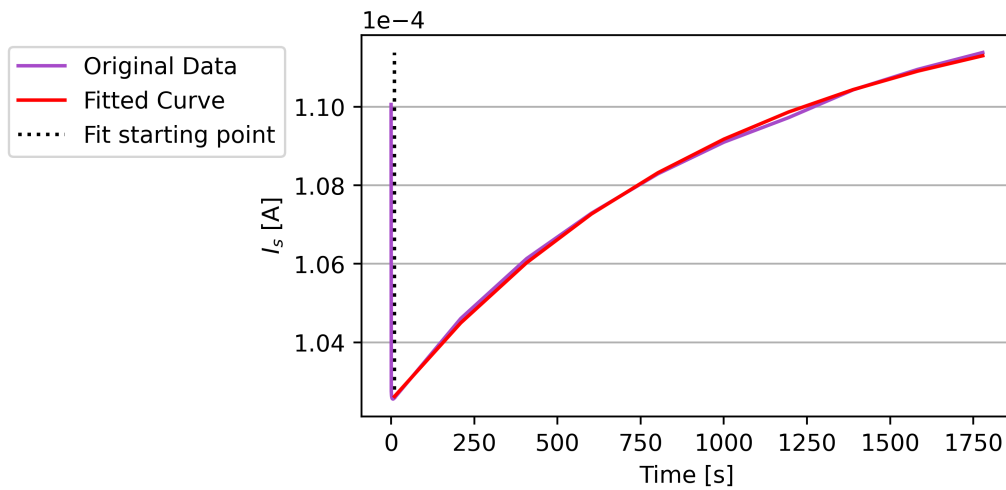
(b) The same experiment as in Figure 4.4a, but now the source- and drain terminals were also disconnected between each measurement.

Figure 4.4

4.2 Solid state electrolyte

The temperature experiment emphasized the inconveniences of water as an electrolyte. Not only does it evaporate, it does also not allow encapsulation, which is found to enhance state retention [11]. In that same source, PEI is added to stabilize the reduced state of PEDOT:PSS. PEI also dissolves out of the PEDOT:PSS in water. For these reasons, the water was replaced with a solid-state electrolyte. This electrolyte consists of the ionic liquid EMIM-TFSI captured in a network of PVDF-HFP.

At first the gel was poured in a mold, allowed to set, cut and pasted onto the ENODes, which produces programmable ENODes. But, for scalability reasons, the gel later on was spincoated at 600 rpm, which yields layers of about 7 micron thick. If spincoated gel also works as an electrolyte, then this is a good step to make the devices more solid-state. The first experiments, both with the patched and spincoated gel, yielded results that were similar to that of water, as can be seen in Figure 4.5. The unevenness in the steps is caused by the sample rate limit of the source-measurement unit used in this measurement that is being reached.
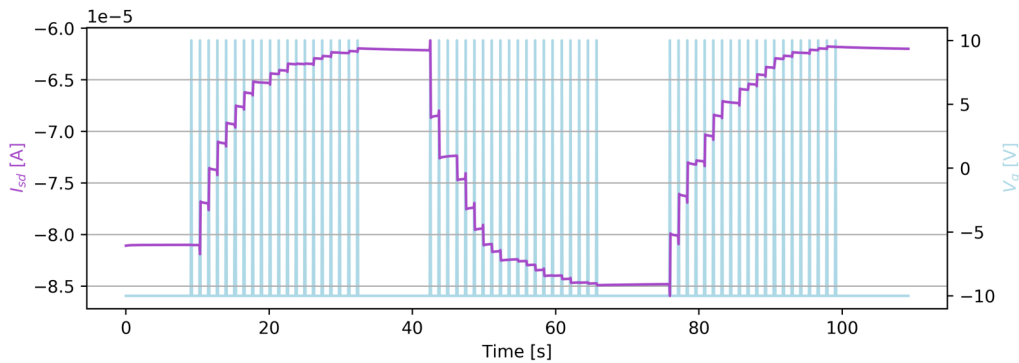
Figure 4.5: Plot of programming measurement with an TFT before the gate, using the setup described in Figure 3.4. This measurement measures the effect of gate pulses on the ENODe channel current. The three sets of pulse trains are respectively positive, negative and positive pulses of (-)0.2V through an open TFT with a resistance of about 10kΩ. This time, however, gel electrolyte was used instead of water. The pulses are 1ms on and 14ms off. The channel voltage is 0.2V.

To explore the possibilities for scaling, a measurement series was done on devices with decreasing channel area. This resulted in a measurement series

that displays the relaxation behaviour of devices with a different channel area, which can be seen in Figure 4.6a. This measurement series was normalized to allow for a better comparison between the relaxations of ENODes of different size, but the original data can be seen in the same figure. In an attempt to quantify this, the same exponent as in Equation 4.1 was fitted to the first 100 seconds of each decay, because that resulted in the best fits. These decay times are plotted in Figure 4.7a, -b and -c against different parameters. The decay time was expected to scale linearly with the ENODe capacitance, which it did not. This will be discussed further in chapter 5. What should also be noted is that generally, a smaller channel has a higher conductivity than a larger channel. This is not entirely expected as the aspect ratio of the channel remains the same, so the sheet resistance should as well. However, the thickness of the channel does not scale with the length, which is likely why the theory of sheet resistance does not hold.
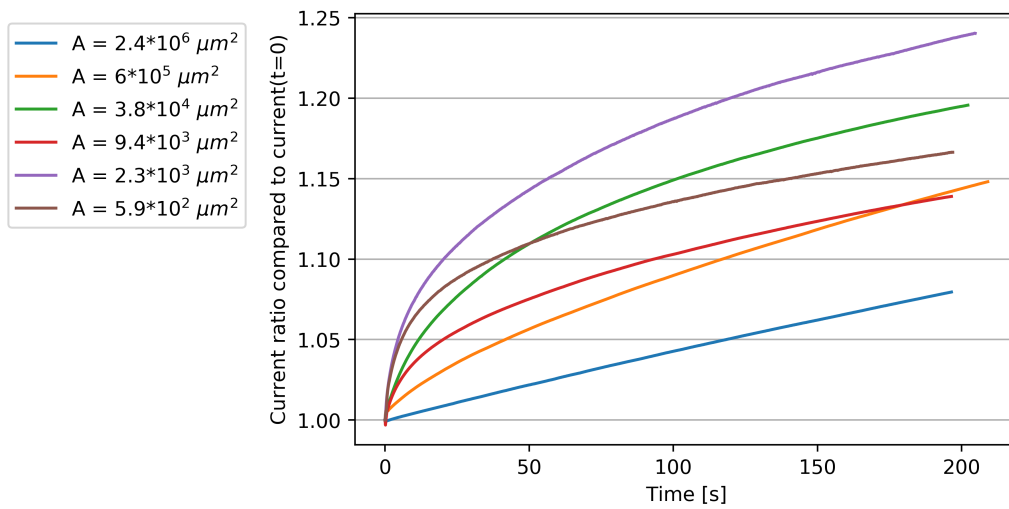
(a) Normalized decay plots of 6 solid-state devices. The samples were all charged at 0.1mV for 10 seconds, after which the gate was disconnected. The channel voltage was 0.1V. The legend indicates the surface area of the channel.
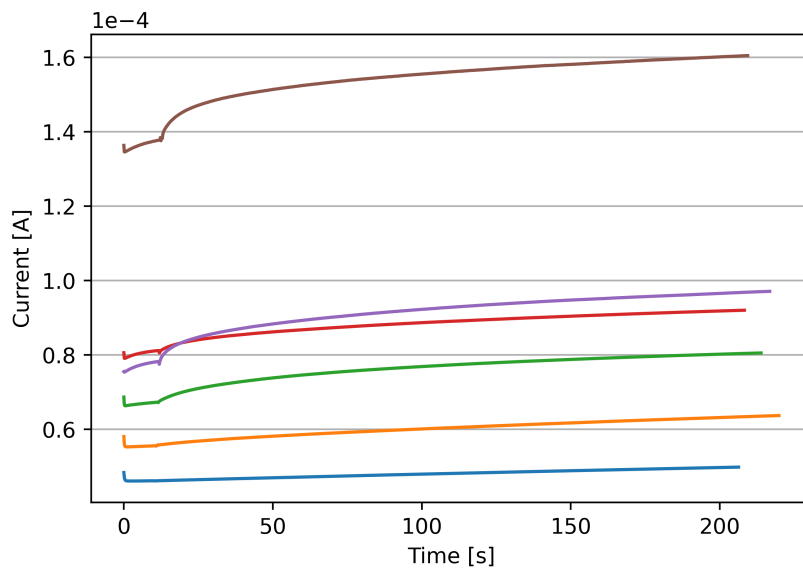
(b) The original data from Figure 4.6a.

Figure 4.6

23
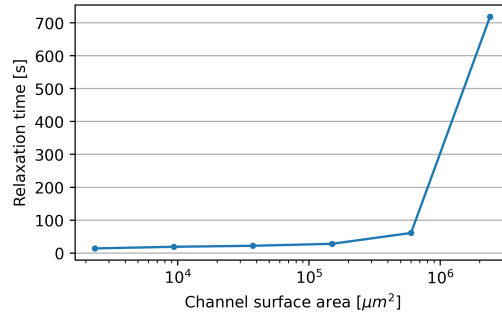
(a) Plot of the exponential decay time fits from Figure 4.6a as a function of channel surface length.
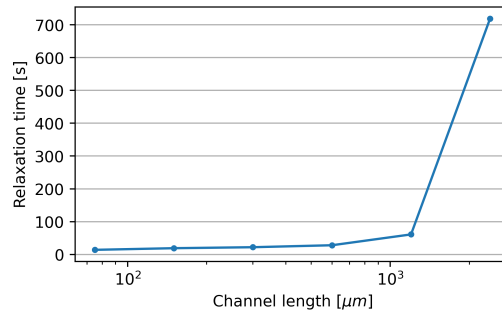
(b) Plot of the exponential decay time fits from Figure 4.6a as a function of channel surface area.
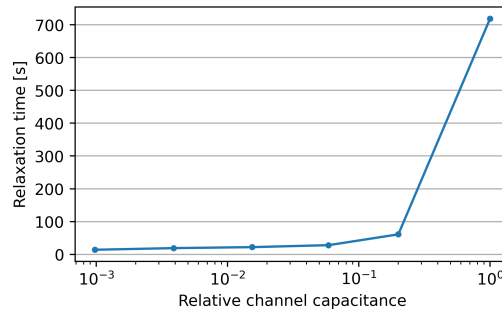
(c) Plot of the exponential decay time fits from Figure 4.6a as a function of total ENODe capacitance, using the calculations from Equation 3.3. The relative capacities are all in relation to the largest ENODe.

Figure 4.7

24

4.3   Drift

The results in the previous section described the effect of scaling the channel and the general trend of the relaxation time were also seen with different electrolytes. One new phenomenon that was not seen in the first of two batches, but was seen in the second is a phenomenon which we classified as drift. Two examples of drift can be seen in Figure 4.8a and -b.

What we consider drift is the change in channel signal except it is different from relaxation. Drift is generally slower and somewhat linear and can be both up- and downwards in direction, though downwards drift is vastly more common.

The drift appears to be influenced by atmosphere, as Figure 4.9b suggests. In that whole measurement series, the device started drifting only after the environment was evacuated and the drift reversed direction once the environment was repressureized. More precisely, the drift appears to be influenced by the exchange of an atmospheric gas like water or oxygen with the electrolyte, and subsequently the exchange with PEDOT:PSS could cause the drift. In order to test this, a device was left inside a glovebox for a month and subsequently measured. This did not erase the drift behaviour, however. Literature also reports a decrease in relaxation [11], but this was not the case for our samples. It took many measurements to isolate a set of data that showed little to no drift, but the fitted relaxation times were similar to those in Figure 4.7a.
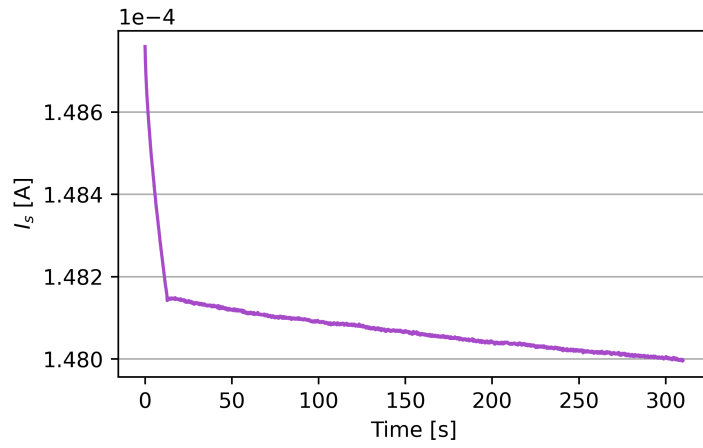
(a) An example of downwards drift. The channel voltage is 0.1V. The device was programmed at 0.1V for 10s and the gate subsequently disconnected.
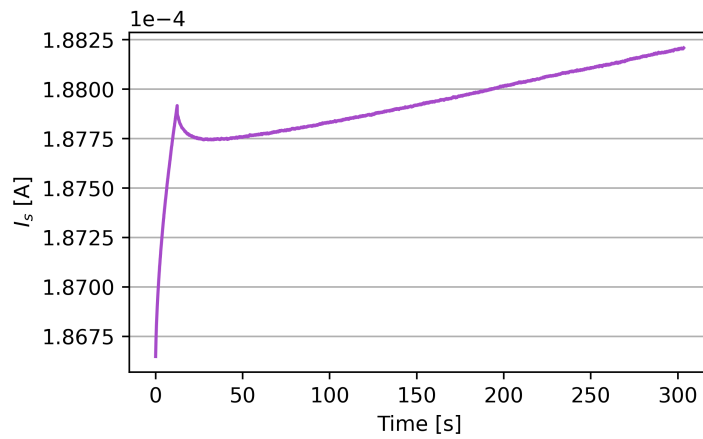
(b) An example of upwards drift. The channel voltage is 0.1V. The device was programmed at 0.1V for 10s and the gate subsequently disconnected.

Figure 4.8

26
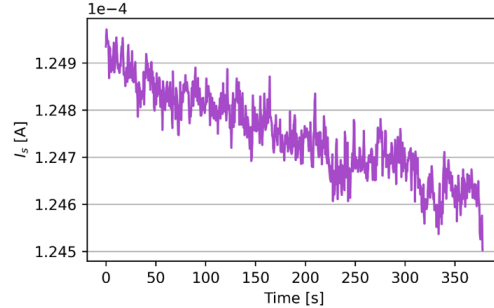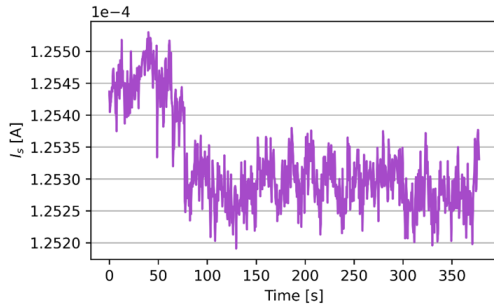
(a) The first measurement in a series. Here, the environment was normal ambient environment. A channel voltage of 0.1V was applied and no gate voltage.

(b) The second measurement in a series. Here, the environment was evacuated shortly before the measurement. A downwards drift appeared in the signal.
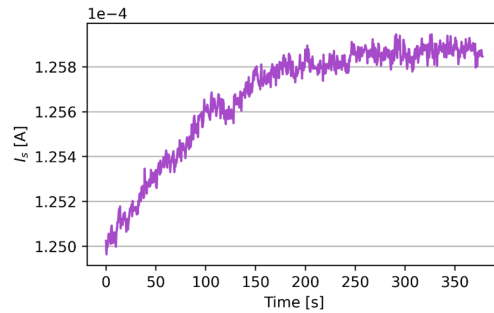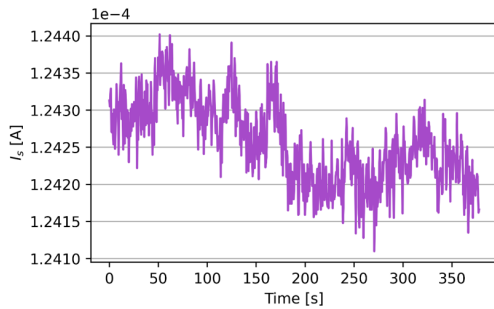
(c) The third measurement in a series. Here, the environment was evacuated for quite a while.

(d) The first measurement in a series. Here, the environment was repressurized right before the measurement. An upwards drift appeared in the signal.

4.4 Encapsulation

In a final attempt to eliminate any exchange with the atmosphere, also any channel-current induced exchange, the devices were encapsulated. A flexible, double-layered barrier was adhered to the device, adhering to- and bending over the gel electrolyte and also adhering to the substrate around the gel. The barrier consisted of an organic layer for mechanical protection and an inorganic layer for protection against moisture. This also did not erase the drift, but it did protect the device. The fact that it did not influence the

workings of the device increases its utility in mass production. It should be noted, however, that two weeks after the encapsulation, a leak was found as one side of the encapsulation released. This still shielded the majority of gel surface area from air, but allowed a few micron wide slit on the side where air could leak.

Another hypothesis is that the PEDOT:PSS is not in an entropically optimal configuration inside the cross-linked network of GOPTS and that either time or current slowly drifts the PEDOT:PSS network into a more favorable configuration. However, multiple measurements taken over the course of five days indicate that there is no trend in the amount of drift over time, as can be seen in Figure 4.10. The direction of the state destabilization switched back and forth with all ENODes of this specific sample over the course of 5 days. This specific sample and these measurements are, however, representable for all data from this batch of samples, in the sense that the behavior of the drift remains mostly unpredictable.
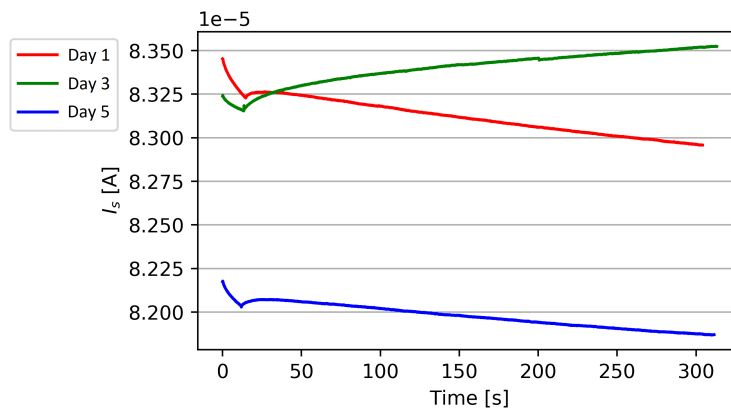

Figure 4.10: Consistency check of an ENODe with a channel surface area of 2.4mm^2. The exact same measurement was done three times, five days apart. On day 1 and 5, drift is visible, whereas it is not on day 3. The devices where charged at 0.1V for 10s, before the gate was disconnected.

28

4.5 Current pulses

The instability issues with the ENODes do not make them unusable. Programming the ENODe with current pulses ensures that the same amount of charge is displaced every time, resulting in a similar dedoping of the channel every pulse. This increases the linear regime significantly, which can be seen in Figure 4.11. There is a trade-off between the amount of occupiable states and lifetime of the states. Since the relaxation is found to be fairly well-described by an exponential decay of the form of Equation 4.1, especially in the earliest phase of the decay, the lifetime of such a state can be approximated by

$$\tau_{state} = \tau * ln(\frac{I_{state} - I_\infty}{I_{state} - I_\infty - \frac{\Delta I}{N}}), \tag{4.2}$$

where

- τ_{state} is the lifetime of a state,

- τ is the characteristic decay time, as plotted in Figure 4.7a,

- I_{state} is the current passing through the channel in that state,

- I_∞ is the equilibrium current reached after the ENODe has completely relaxed,

- ΔI is the difference between the maximum- and minimum achievable channel current, also defined as the programming range and

- N is the amount of states the programmer divided the programming range into.
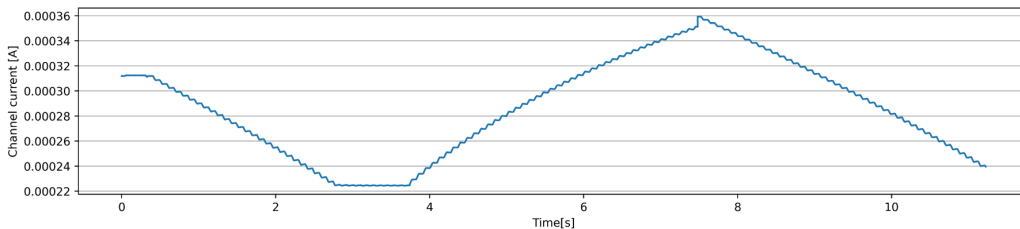
Figure 4.11: Plot of a programming cycle using current pulses on a device with a surface area of 2.4mm^2. With every 10ms pulse, 30nC was supplied to the gate, which has a capacity of roughly 2 μF. The time between two pulses is 30 ms.

The derivation of this formula will be given in chapter 6. One should be careful with current pulses as sourcing a certain current may require extensive voltage to be sourced over the channel. Prolonged subjection to voltages of over 300 mV have been found to alter the devices. The ENODe gates have a capacitance in the order of μF. An example of this can be seen in Figure 5.1. During the programming, the current increased while it was expected to decrease, meaning that it moved closer to the equilibrium state without the operators intention. This is assumed to be caused by alterations to the PEDOT:PSS morphology. There are things that can be done to improve these devices, which will be discussed in the next chapter. This concludes the results chapter. The conclusions and discussion will also follow in the next chapter.

Chapter 5

Conclusion and Discussion

The two main obstacles for state retention are relaxation and drift. The relaxation time decreases with decreasing channel area, which is an obstacle to keep in mind when downsizing the devices, which would ultimately become preferable for mass production and space-efficient hardware.

The actual relation between relaxation and channel dimensions is not entirely as expected. It is expected that a smaller channel has a smaller ion capacity, which indeed leads to a shorter relaxation time as expected, but the relaxation time does not scale linearly with the ENODe capacitance. There are a couple of explanations for this discrepancy. The most evident explanation is the exponential fits do consistently not fit perfectly over the relaxation decay, an example of which can be seen in Figure 5.1. This difference between fit and measurement is the largest for the smallest devices. Another explanation is that the ions do not occupy the PEDOT:PSS like electrons occupy a capacitor. The mobility of ions through a complex, cross-linked network of PEDOT:PSS and across the PEDOT:PSS - electrolyte interface is a very difficult mechanism to quantify. The third explanation is a design error. In decreasing the channel size, the distance between the channel and gate increases with each subsequent ENODe on a sample. The increased distance the cations have to diffuse over could very well influence the relaxation time.

The drift remains ill-understood. What is certain is that only devices from the last batch show this behavior. The difference with the previous batch is that this batch has the surfactant DBSA added to help with the adhesion of the PEDOT:PSS to the substrate. However, other groups have tried and tested this addition and not reported the same issues.

The encapsulation did not change the behavior of the ENODes. This, on the one hand, is beneficial for the prospect of mass production. It did, however, not reduce the relaxation nor drift, which is not in agreement with

literature [11]. This could be because of the leak in the encapsulation, even though the majority of the surface area was covered by the barrier. This should at least delay the relaxation to a small degree.

Even more so, the devices left in the glove box for a month did still not show a delayed relaxation or lack of drift, the first of which is also not in agreement with literature [11]. In that paper, the inert nitrogen environment prevented any reactions with oxygen or water. It did not address the back diffusion of cations, which is what we assume is the remaining relaxation mechanism. What has been found to delay this back diffusion is disconnecting the source- and drain terminals to prevent compensating terminal charges from flowing in and compensating the lack of cations.

Using current pulses instead of voltage pulses increased the linear regime in the programming range and the formula for state lifetimes provides guidance in what is achievable with the current ENODe technology. The next steps that could be made include:

- Adding PEI to the channel PEDOT:PSS to stabilize the reduced state of PEDOT:PSS,

- a different solid-state electrolyte to see if it inhibits back-diffusion, for example Nafion with KCl or

- a different form of encapsulation, for example a glass plate over the electrolyte with epoxy along the sides,

as other groups have reported these methods to enhance state retention [11]. The current attention this technology has and the vast amount of possibilities that its main- and spin-off applications have make ENODes a promising field. Of course, the viability for Holst Centre lies in the expected costs for this further research. With this advice, we conclude the report.
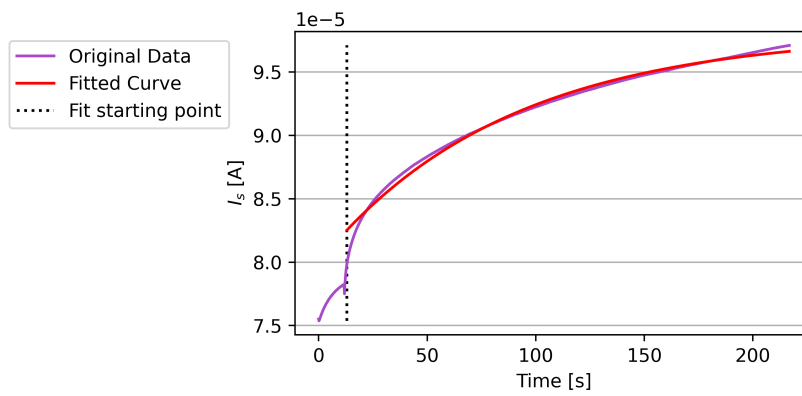
Figure 5.1: An example of a fit that does not fit well to the measurement. Also an example of a programming voltage raising the channel conductance instead of lowering it, as can be seen in the programming phase before t=10s.

Bibliography

[1] Wenjun Zhang and Albert Barrion. Function approximation and documentation of sampling data using artificial neural networks. *Environmental monitoring and assessment*, 122(1):185–201, 2006.

[2] Richard P Lippmann. Pattern classification using neural networks. *IEEE communications magazine*, 27(11):47–50, 1989.

[3] TB Blank and SD Brown. Data processing using neural networks. *Analytica chimica acta*, 277(2):273–287, 1993.

[4] CT Harsten. Application of neural networks to robotics. *Handbook of Neural Computing Applications*, pages 381–389, 1990.

[5] Pooneh Safayenikoo and Ismail Akturk. Weight update skipping: Reducing training time for artificial neural networks. *arXiv preprint arXiv:2012.02792*, 2020.

[6] Norm Jouppi. Google supercharges machine learning tasks with tpu custom chip.

[7] Yoeri van de Burgt, Ewout Lubberman, Elliot J Fuller, Scott T Keene, Grégorio C Faria, Sapan Agarwal, Matthew J Marinella, A Alec Talin, and Alberto Salleo. A non-volatile organic electrochemical device as a low-voltage artificial synapse for neuromorphic computing. *Nature materials*, 16(4):414–418, 2017.

[8] Scott T Keene, Armantas Melianas, Elliot J Fuller, Yoeri van de Burgt, A Alec Talin, and Alberto Salleo. Optimized pulsed write schemes improve linearity and write speed for low-power organic neuromorphic devices. *Journal of Physics D: Applied Physics*, 51(22):224002, 2018.

[9] Paschalis Gkoupidenis, Nathan Schaefer, Benjamin Garlan, and George G Malliaras. Neuromorphic functions in pedot: Pss organic electrochemical transistors. *Advanced Materials*, 27(44):7176–7180, 2015.

[10] Paschalis Gkoupidenis, Dimitrios A Koutsouras, and George G Malliaras. Neuromorphic device architectures with global connectivity through electrolyte gating. *Nature communications*, 8(1):1–8, 2017.

[11] Scott Tom Keene, Armantas Melianas, Yoeri van de Burgt, and Alberto Salleo. Mechanisms for enhanced state retention and stability in redox-gated organic neuromorphic devices. *Advanced Electronic Materials*, 5(2):1800686, 2019.

[12] Yoeri van De Burgt, Armantas Melianas, Scott Tom Keene, George Malliaras, and Alberto Salleo. Organic electronics for neuromorphic computing. *Nature Electronics*, 1(7):386–397, 2018.

[13] Matteo Ghittorelli, Leona Lingstedt, Paolo Romele, N Irina Crăciun, Zsolt Miklós Kovács-Vajna, Paul WM Blom, and Fabrizio Torricelli. High-sensitivity ion detection at low voltages with current-driven organic electrochemical transistors. *Nature communications*, 9(1):1–10, 2018.

[14] Paschalis Gkoupidenis, Nathan Schaefer, Xenofon Strakosas, Jessamyn A Fairfield, and George G Malliaras. Synaptic plasticity functions in an organic electrochemical transistor. *Applied Physics Letters*, 107(26):263302, 2015.

[15] Dimitrios A Koutsouras, George G Malliaras, and Paschalis Gkoupidenis. Emulating homeoplasticity phenomena with organic electrochemical devices. *MRS Communications*, 8(2):493–497, 2018.

[16] Leona V Lingstedt, Matteo Ghittorelli, Maximilian Brückner, Jonas Reinholz, N Irina Crăciun, Fabrizio Torricelli, Volker Mailänder, Paschalis Gkoupidenis, and Paul WM Blom. Monitoring of cell layer integrity with a current-driven organic electrochemical transistor. *Advanced healthcare materials*, 8(16):1900128, 2019.

[17] Leona V Lingstedt, Matteo Ghittorelli, Hao Lu, Dimitrios A Koutsouras, Tomasz Marszalek, Fabrizio Torricelli, N Irina Crăciun, Paschalis Gkoupidenis, and Paul WM Blom. Effect of dmso solvent treatments on the performance of pedot: Pss based organic electrochemical transistors. *Advanced Electronic Materials*, 5(3):1800804, 2019.

[18] Luis Alcácer. Case study: Pedot:pss. In *Electronic Structure of Organic Semiconductors*, 2053-2571, pages 9–1 to 9–15. Morgan & Claypool Publishers, 2018.

[19] Anton V Volkov, Kosala Wijeratne, Evangelia Mitraka, Ujwala Ail, Dan Zhao, Klas Tybrandt, Jens Wenzel Andreasen, Magnus Berggren, Xavier Crispin, and Igor V Zozoulenko. Understanding the capacitance of pedot: Pss. *Advanced Functional Materials*, 27(28):1700329, 2017.

Chapter 6

Appendix

6.1 TFT transfer curve
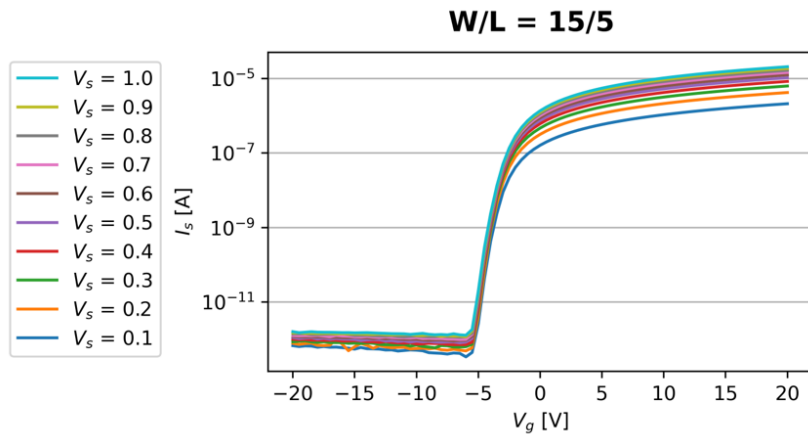

Figure 6.1: Transfer curve of a IGZO-TFT with W/L=15/5.

6.2 Derivation of state lifetime formula

By approximation, the decay of the programmed state of an ENODe follows an exponential decay. The decay does not decay back to 0. Taking into account the boundary condition that the decay should begin at the initial level and decay to the equilibrium level, we get

$$I(t) = (I_0 - I_\infty)e^{-\frac{t}{\tau}} + I_\infty. \tag{6.1}$$

after a time τ_s, the current will have decayed to a current that is one state apart. The size of a state is $\frac{\Delta I}{N}$, where ΔI is the total programmable range and N the amount of states the programmer wishes to occupy, so

$$I_{state} - \frac{\Delta I}{N} = (I_{state} - I_\infty)e^{-\frac{\tau_s}{\tau}} + I_\infty \qquad (6.2)$$

.

Now it is only a matter of isolating τ_{state}, which leads to

$$\tau_{state} = \tau * ln(\frac{I_{state} - I_\infty}{I_{state} - I_\infty - \frac{\Delta I}{N}}), \qquad (6.3)$$

where

- τ_{state} is the lifetime of a state,

- τ is the characteristic decay time,

- I_{state} is the current passing through the channel in that state,

- I_∞ is the equilibrium current reached after the ENODe has completely relaxed,

- ΔI is the difference between the maximum- and minimum achievable channel current, also defined as the programming range and

- N is the amount of states the programmer divided the programming range in.